A TRIDENT SCHOLAR PROJECT REPORT

NO. 536

Quantum Engineering in the Undergraduate Laboratory: Tests and Violations of Local Realism

by

Midshipman 1/C Robert L. Hare, USN

UNITED STATES NAVAL ACADEMY
ANNAPOLIS, MARYLAND

USNA-1531-2

REPORT DOCUMENTATION PAGE

Form Approved
OMB No. 0704-0188

1. REPORT DATE *(DD-MM-YYYY)*	**2. REPORT TYPE**	**3. DATES COVERED** *(From - To)*
5-16-23		

4. TITLE AND SUBTITLE

Quantum Engineering in the Undergraduate Laboratory: Tests and Violations of Local Realism

5a. CONTRACT NUMBER

5b. GRANT NUMBER

5c. PROGRAM ELEMENT NUMBER

6. AUTHOR(S)
Robert L. Hare

5d. PROJECT NUMBER

5e. TASK NUMBER

5f. WORK UNIT NUMBER

7. PERFORMING ORGANIZATION NAME(S) AND ADDRESS(ES)

8. PERFORMING ORGANIZATION REPORT NUMBER

9. SPONSORING / MONITORING AGENCY NAME(S) AND ADDRESS(ES)
U.S. Naval Academy
Annapolis, MD 21402

10. SPONSOR/MONITOR'S ACRONYM(S)

11. SPONSOR/MONITOR'S REPORT NUMBER(S)
Trident Scholar Report no. 536 (2023)

12. DISTRIBUTION / AVAILABILITY STATEMENT

This document has been approved for public release; its distribution is UNLIMITED.

13. SUPPLEMENTARY NOTES

14. ABSTRACT

The application of quantum mechanics to computing, communication, and sensing may constitute a revolution in technology. Furthermore, the field of quantum foundations has experienced high-profile success, especially in recent years, prompting the need to provide exposure to applied quantum engineering at the undergraduate level in order to ensure the development of a "quantum workforce." Entanglement is a critical aspect of quantum technology and is fundamental to quantum foundations, but entangled systems behave in strange ways. Classical systems behave in accordance with the concepts put forth by local realism, which characterizes systems as only being affected by their surroundings and that this influence cannot travel faster than the speed of light, as well as that properties of such a system are real and exist independent of a measurement made on those properties. Quantum systems, on the other hand, do not abide by the concepts of local realism and often behave in strange ways that are counter-intuitive to our classical view of the world. This project analyzes the behavior of entangled systems and the concepts of local realism through experimental verification. The initial phase of this project builds and characterizes the first entangled photon source available to undergraduates at the United States Naval Academy. Utilizing the techniques of spontaneous parametric down-conversion, we have built a high luminosity source of entangled photons integrated to optical fiber and characterized with modular single photon avalanche photodiodes. The final phase of this project conducts tests of local realism set forth by John Glauser and Alain Aspect. The primary focus of this phase is a test of the CHSH inequality as an experimentally accessible test of Bell's theorem. We use this test of local realism to further characterize the system and enable future exploration in applications of quantum information science, such as quantum computing and quantum cryptography.

15. SUBJECT TERMS
Quantum foundations, Local realism, Bell's Inequality

16. SECURITY CLASSIFICATION OF:			**17. LIMITATION OF ABSTRACT**	**18. NUMBER OF PAGES**	**19a. NAME OF RESPONSIBLE PERSON**
a. REPORT	**b. ABSTRACT**	**c. THIS PAGE**		20	**19b. TELEPHONE NUMBER** *(include area code)*

U.S.N.A. --- Trident Scholar project report; no. 536 (2023)

QUANTUM ENGINEERING IN THE UNDERGRADUATE LABORATORY: TESTS AND VIOLATIONS OF LOCAL REALISM

by

Midshipman 1/C Robert L. Hare
United States Naval Academy
Annapolis, Maryland

Certification of Adviser(s) Approval

Associate Professor Seth T. Rittenhouse
Physics Department

Associate Professor Joel Helton
Physics Department

CDR Michael Manicchia, USN
Associate Chair, Physics Department

Acceptance for the Trident Scholar Committee

Professor Maria J. Schroeder
Associate Director of Midshipman Research

USNA-1531-2

Quantum Engineering in the Undergraduate Laboratory: Tests and Violations of Local Realism

MIDN 1/C Robert Hare,[1] Dr. Peter Brereton,[2] Dr. Seth Rittenhouse,[1] Dr. Joel Helton,[1] and CDR Michael Manicchia, USN[1]

[1]*Department of Physics, United States Naval Academy, Annapolis, Maryland 21402 USA*
[2]*Goddard Space Flight Center*

(Dated: 10 May 2023)

Abstract: The application of quantum mechanics to computing, communication, and sensing may constitute a revolution in technology. Furthermore, the field of quantum foundations has experienced high-profile success, especially in recent years, prompting the need to provide exposure to applied quantum engineering at the undergraduate level in order to ensure the development of a "quantum workforce." Entanglement is a critical aspect of quantum technology and is fundamental to quantum foundations, but entangled systems behave in strange ways. Classical systems behave in accordance with the concepts put forth by local realism, which characterizes systems as only being affected by their surroundings and that this influence cannot travel faster than the speed of light, as well as that properties of such a system are real and exist independent of a measurement made on those properties. Quantum systems, on the other hand, do not abide by the concepts of local realism and often behave in strange ways that are counter-intuitive to our classical view of the world. This project analyzes the behavior of entangled systems and the concepts of local realism through experimental verification. The initial phase of this project builds and characterizes the first entangled photon source available to undergraduates at the United States Naval Academy. Utilizing the techniques of spontaneous parametric down-conversion, we have built a high luminosity source of entangled photons integrated to optical fiber and characterized with modular single photon avalanche photodiodes. The final phase of this project conducts tests of local realism set forth by John Clauser and Alain Aspect. The primary focus of this phase is a test of the CHSH inequality as an experimentally accessible test of Bell's theorem. We use this test of local realism to further characterize the system and enable future exploration in applications of quantum information science, such as quantum computing and quantum cryptography.

Keywords: *quantum foundations, local realism, Bell's inequality*

Contents

I. INTRODUCTION

Many of the fundamental concepts in quantum mechanics have been around since the beginning of the 20th century and are well-established through theory and experiment. However, many of these principles and properties are counter-intuitive to those in classical mechanics. Attempts to further understand and explain why quantum systems behave in these ways is studied in a field called quantum foundations. These concepts have been mathematically and experimentally verified and more publicly validated by the winning of the Nobel Prize in physics last year by John Clauser, Alain Aspect, and Anton Zeilinger, three of the most prominent physicists that have explored these ideas in the past 60 years [1, 2].

Entanglement is one of the characteristics of quantum mechanics that fundamentally differentiates it from classical physics. Questions regarding this strange behavior dates back all the way to 1935 with the publishing of the paper "Can Quantum-Mechanical Description of Physical Reality be Considered Complete?" by Albert Einstein, Boris Podolsky, and Nathan Rosen [3]. In that paper, they proposed a paradox (the "EPR paradox") which sought to assert that the theory of quantum mechanics was incomplete as these systems seemed to behave in contrast with the ideas of local realism [4]. 'Locality' is the notion that measurements performed in one part of a system do not, and cannot, affect measurement outcomes in other parts of the system. 'Realism' is the concept that aspects of a system that can be measured have values for those measurable quantities, whether or not they have actually been measured. 'Local realism' specifically is the combination of both of these ideas, and we can see examples of this in numerous classical systems. The EPR paradox sought to find a deterministic theory of quantum mechanics, and argued that, if there was no deterministic theory, the quantum-mechanical description of the universe must therefore be incomplete. This prompted John Bell to assume the existence of 'local hidden variables' within entangled systems and explore the mathematical implications on such systems. These variables would account for any information that would make the system deterministic regarding the observables within that system, and Bell concluded that, if the existence of 'local hidden variables' was true, a certain combination of measurements that could be made on any system should abide by an inequality deemed "Bell's inequality" [5].

Studying the behavior of entangled systems allows for exploration into the ideas of quantum foundations. This paper describes the theory of local realism and Bell's theorem, then discusses the CHSH inequality as well as its associated test. The design of the experiment conducted to measure the entangled state initially generated for the CHSH test of local realism is presented along with a discussion of the characterization of the experimental apparatus. Subsequently, there is a brief discussion of another test of local realism – the Hardy test – in which we slightly modified our apparatus in order to verify, in a different way, the same conclusion as the CHSH test of local realism. Attached as appendices are a derivation of Bell's inequality, a derivation of the CHSH inequality and a discussion of an undergraduate lab development done in conjunction with another Midshipman as a senior capstone at the United States Naval Academy.

II. LOCAL REALISM, HIDDEN VARIABLES, AND BELL'S INEQUALITY

The *gedankenexperiment* put forth in 1935 by Albert Einstein, Boris Podolsky and Nathan Rosen, more commonly referred to as the "EPR Paradox," questioned whether the theory of quantum mechanics could be considered complete due to the behavior of entangled systems. When discussing classical systems, many ideas seem intuitive and fundamental to the way our world works. One of these concepts is "local realism," which asserts two fundamental realities: The first that results of measurements on one part of a system do not affect the outcomes of measurements on a different part of the same system, and second that properties being measured are definite, regardless of the act of measuring the property itself [6]. However, because entangled states behave in a probabilistic and correlative manner, Einstein, Podolsky and Rosen posited that either quantum mechanical theory was incomplete or the correlation between measurements of entangled states cannot be a "simultaneous reality."

Einstein believed the theory could only be considered complete if "every element of ... physical reality [has] a counterpart in the physical theory" [3] Einstein's conceptual solution to this 'incomplete' aspect of the theory was "local hidden variables." This theory, referred to as "local hidden variable theory," accounts for the correlation in measurement outcomes of entangled states by concluding that there are variables (one or more) that are causing this correlation that, if we knew what they were or had access to that information of the system, we could understand quantum systems in a more deterministic way.

The EPR paper resulted in the mathematical exploration of 'local hidden variable theory' by John Bell in the 1960s. Bell began his work by asking himself the question, "Does local hidden variable theory have mathematical consequences?" He started with the assumption of the existence of local hidden variables and ultimately found that there are mathematical limitations on the measurements of correlated (or entangled) systems in accordance with an underlying existence of local hidden variables. His work resulted in the development of the following expression,

known as "Bell's inequality," which is derived in further detail in Appendix A [5]:

$$\left|E(\vec{a},\vec{b}) - E(\vec{a},\vec{c})\right| \leq 1 + E(\vec{b},\vec{c}) \tag{1}$$

where E is the "expectation value" – the average of all possible measurement outcomes of a state weighted with their likelihood of occurring. A simple way to think of Bell's inequality is using areas to represent the relevant probabilities, the accompanying figure for which is shown in Figure 1 [7].

Let us define three properties that can be measured in a two-object system with the corresponding outcomes, where A is a measurement on object one and B and C are measurements made on object two:

$$A = \pm 1,\ B = \pm 1,\ C = \pm 1 \tag{2}$$

The probability that A and B are measured to be the same is given by $P_{same}(A,B)$, and the probability they are different as $P_{diff}(A,B)$. It is obvious that the sum of these probabilities would be one, as either A and B are the same or different, shown mathematically in Equation (3) and as an image in Figure 1(a).

$$P_{same}(A,B) + P_{diff}(A,B) = 1 \tag{3}$$

If we were to then take into account property C, there is a probability associated with C being the same or different as A. However, when considering all three properties, it is possible that A, B, and C are all the same – the overlap in the $P_{same}(A,B)$ and $P_{same}(A,C)$ circles (dashed and solid, respectively) in Figure 1(b). As a consequence, if we were to look at the probability that B and C are the same, we would see that there is a higher probability of that than the probability of A being different from both B and C:

$$P_{same}(B,C) \geq P_{diff}(A, B\,\&\,C) \tag{4}$$

Consequently, we can conclude that summing the probabilities of measuring two properties to be the same would be greater than one as follows:

$$P_{same}(A,B) + P_{same}(A,C) + P_{same}(B,C) \geq 1 \tag{5}$$

The above inequality holds if the properties and measurements thereof are consistent with local realism. The essential takeaway is that, assuming measurements made on one part of a system do not affect measurements another part of a system or the reality of those measurements before they are actually made, there are certain mathematical expressions that must hold.

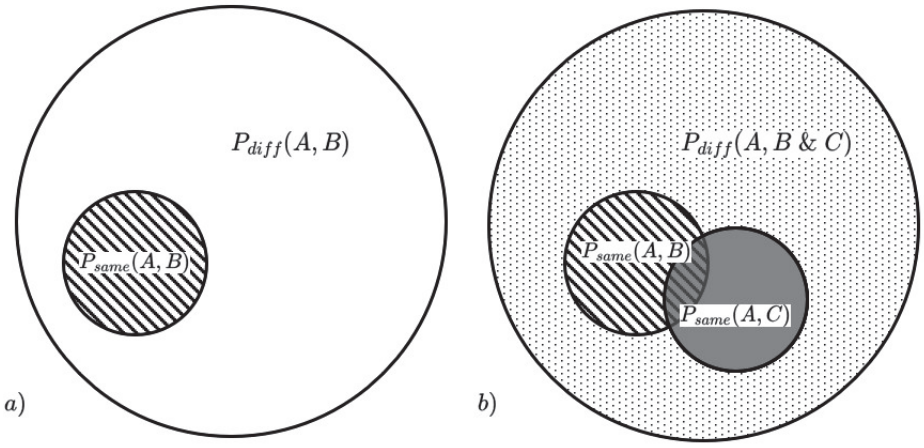

FIG. 1: Reference images for discussion of simple explanation of Bell's theorem where the areas of circles represent probabilities. (a) The probability that A and B are the same, $P_{same}(A,B)$, and the probability that A and B are different, $P_{diff}(A,B)$, sum to 1 as in Equation (3) (i.e. the areas sum to the total area of the circle). (b) The small, dashed circle represents the probability that A and B are the same ($P_{same}(A,B)$), and the small, solid gray circle represents the probability that A and C are the same ($P_{same}(A,C)$). The rest of the circle represents the probability that A is different from B and C ($P_{diff}(A, B\,\&\,C)$).

III. CHSH INEQUALITY

A. Background and Theory of the CHSH Inequality

In 1969, John Clauser, Michael Horne, Abner Shimony, and Richard Holt published a paper proposing an experiment that could test local hidden variable theories. They produced an experimentally-accessible variation of Bell's inequality known as the Clauser-Horne-Shimony-Holt (CHSH) inequality [1]. Instead of an experiment involving the spin of entangled particles, the CHSH test of local realism generates polarization entangled photons and makes measurements on that system to determine whether or not quantum mechanics and quantum systems are compatible with local hidden variable theory or abide by local realism.

The proposed experiment redefined the 'correlation function' from Bell's inequality, $E(\vec{a}, \vec{b})$, in order for it to only depend on the relative angle between $\vec{a}$ and $\vec{b}$. This gives the CHSH inequality as:

$$E(b - b') + E(b' - c) + |E(b - a) - E(a - c)| \leq 2 \tag{6}$$

where, again, E is the expectation value of a state with the parameters indicated in parentheses and has possible values ranging from -1 to 1. They also found that quantum mechanical theory predicted that, for an entangled state in an equal superposition of horizontally and vertically polarized photon pairs, a maximum violation of this inequality at the relative orientations of 22.5° and 67.5°.

More simply put for the sake of this experiment, we can define the parameter S as:

$$S \equiv E(\theta_{A1}, \theta_{B1}) + E(\theta_{A2}, \theta_{B1}) - E(\theta_{A2}, \theta_{B2}) + E(\theta_{A1}, \theta_{B2}) \tag{7}$$

In Equation (7), S is in terms of the expectation value of measurements made and are dependent on the relative angle of the parameters, and these expectation values depend on the relative angle of θ_A and θ_B [6]. The subscripts correspond to the angles at which the adjustable optics are set in the detection portion of our apparatus(in our case it is two half-wave plates, discussed in detail in Section III(D); e.g. $E(\theta_{A1}, \theta_{B1})$ is the expectation value when the adjustable optic along the first output beam path is set to θ_{A1} and the adjustable optic along the second output beam path is set to θ_{B1}, and $E(\theta_{A2}, \theta_{B2})$ is the expectation value when the adjustable optics are set to θ_{A2} and θ_{B2}, and so on). In this version, the quantity S is bound by the following inequality:

$$|S| \leq 2 \tag{8}$$

An entangled state in an equal superposition of horizontally and vertically polarized photon pairs ($|H\rangle |H\rangle$ and $|V\rangle |V\rangle$), as discussed in the CHSH paper, is represented with the following equation:

$$|\psi\rangle = \frac{1}{\sqrt{2}} \left(|H\rangle_A |H\rangle_B + |V\rangle_A |V\rangle_B \right) \tag{9}$$

The expectation value of this state as a function of θ_A and θ_B is:

$$E(\theta_A, \theta_B) = \cos 2(\theta_A - \theta_B) \tag{10}$$

To illustrate an example of adhering to local realism, we could set the four angles to the following angles in order to understand how some measurements on these states would calculate S: $\theta_{A1} = 0°$, $\theta_{A2} = 45°$, $\theta_{B1} = 0°$, and $\theta_{B2} = 90°$. In this example, we see that each expectation value is either $+1$, 0, or -1. This gives a calculation of S as follows:

$$S = E(0°, 0°) + E(45°, 0°) - E(45°, 90°) + E(0°, 90°) = 1 + 0 - 0 + (-1) = 0 \tag{11}$$

As we can see, at the above angle parameters, S turns out to be 0, abiding by the inequality from Equation (8) as it falls between -2 and 2.

However, when we see a deviation from these theory when we set the angle parameters to the following settings:

$$\theta_{A1} = 0^\circ,\ \theta_{A2} = 45^\circ,\ \theta_{B1} = 22.5^\circ,\ \theta_{B2} = -22.5^\circ$$

These parameters agree with Clauser's prediction of a maximal violation of local realism because these relative angles are

$$\theta_{B1} - \theta_{A1} = \theta_{A2} - \theta_{B1} = \theta_{A1} - \theta_{B2} = 22.5^\circ$$
$$\theta_{A2} - \theta_{B2} = 67.5^\circ$$

These parameters, in theory, yield a maximum S value of $S = 2\sqrt{2}$, which violates the CHSH inequality. This means that the observed correlation in measurement outcomes in entangled systems cannot be attributed to the 'hidden variables' as suggested by Einstein.

B. Experimentally Generating an Entangled State

In order to analyze these systems, we had to create an apparatus that generates entangled states and properly analyzes and measures those states. A brief overview of the apparatus is given in the following paragraphs, and there are more in-depth descriptions in the following subsections.

In order to generate polarization entangled photons, we built an apparatus that utilizes spontaneous parametric downconversion (SPDC) and single photon detection. In order to generate an entangled state, we use two BBO crystals (DC in Figure 2) placed back-to-back with orthogonal polarization directions, one oriented vertically and the other horizontally, and pump that crystal pair with 405 nm light (at a current of 100 mA from the power source). If the half-wave plate ($\lambda/2$ in Figure 2) is placed at 22.5°, we generate the following state:

$$|\psi\rangle = \frac{1}{\sqrt{2}}\left(|H\rangle_A |H\rangle_B + e^{i\phi} |V\rangle_A |V\rangle_B\right) \tag{12}$$

The phase shift in Equation (12) is due to the physical space between the two BBO crystals. In order to account for this difference, we place a birefringent plate (BP in Figure 2) in between the half-wave plate and the SPDC crystal pair and adjust it accordingly until we properly tune the apparatus to our desired state, generating the intended entangled state below:

$$|\psi\rangle = \frac{1}{\sqrt{2}}\left(|H\rangle_A |H\rangle_B + |V\rangle_A |V\rangle_B\right) \tag{13}$$

Simply put, the above state is one in which there is an equal probability of measuring horizontally- or vertically-polarized photon pairs. The individual photons and coincident counts are measured using single photon avalanche photodiodes (SPAPDs). The measurement parameters are such that that incident photons are considered "entangled" (or are considered a "photon pair") if the two photons are detected within 10 nanoseconds in a given SPAPD pair (e.g. AB, AB', $A'B$, and $A'B'$). These pairs, referred to in this project as "coincidence counts," are then summed over one second in order to calculate the associated probabilities and expectation values.

C. Generating Entanglement in the Apparatus

This apparatus generates polarization entangled photons via spontaneous parametric downconversion. In this technique, pairs of photons are produced through a non-linear optical effect that occurs when crystalline materials that lack an inversion center are irradiated with intense laser light, called the 'pump beam.' The oscillating electrons re-emit light only at frequencies and directions in which the input and output phases are matched. Of particular concern is that this process can produce an output of two beams – with half of the wavelength – centered around the pump beam. In our setup, the non-linear optical crystal is β-barium borate (BBO) in the Type I alignment. This means that, when pumped with an intense 405 nm laser with a given polarization, the crystal will produce "twin" beams of 810 nm light arranged symmetrically 3° on either side of the pump beam direction. These down-converted photons have identical polarization axes.

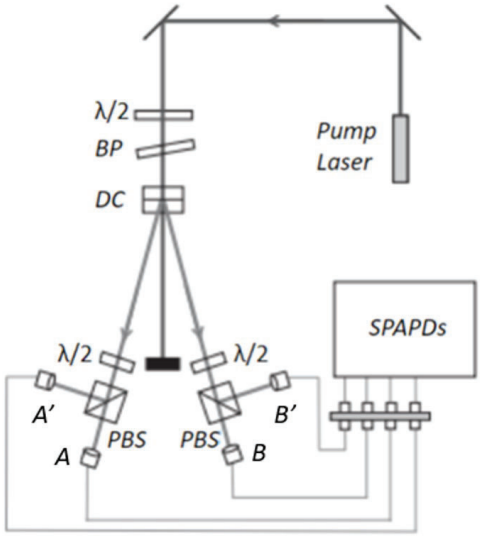

FIG. 2: Schematic of the apparatus utilized in this project. A half-wave plate ($\lambda/2$) is placed in front of a birefringent plate (BP) in order to pump the downconversion crystal pair (DC) and generate the desired entangled state. In order to measure and detect the entangled photons, there are four detectors (A, A', B, and B') which are linked with fiber optic cables to single photon avalanche photodiodes ($SPAPDs$) [6].

In this case, the pump beam is a laser with a wavelength of 405 nm. We collimate the light in order to focus the pump beam into the downconversion crystals and maximize the SPDC effect. This is achieved by a series of lenses and mirrors, shown in Figure 3, that allows us to take the initial, unchanged laser beam and minimize the divergence of the beam.

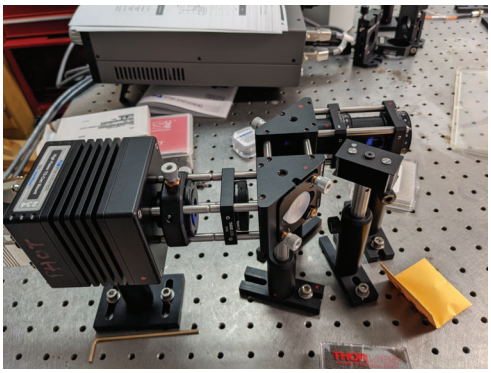

FIG. 3: Front-end of the apparatus which collimates the pump light at 405 nm and focuses it into the initial half-wave plate.

The collimated light then goes through a half-wave plate. A half-wave plate allows for the rotation of the polarization of input light without affecting the intensity of the pump light. To generate the state from Equation (13), we set the half-wave plate to an angle of 22.5°. After the half-wave plate, the light goes through a birefringent plate and the downconversion crystals, as shown in Figure 4. A consequence of spontaneous parametric downconversion is that the two output beams of 810 nm light are polarized along the same axis as the downconversion crystal through which they passed. Thus, we place one horizontally-oriented BBO crystal back-to-back with a vertically-oriented BBO crystal in order to generate an equal superposition of horizontally and vertically polarized photons in the two output beams. One note is that the difference in physical location of the two BBO downconversion crystals, which is only a couple of millimeters, causes a slight misalignment of the output beams from each individual crystal. To account for this, the birefringent plate allows us to adjust the relative phase shift of each beam in order to match the output beams of light for detection.

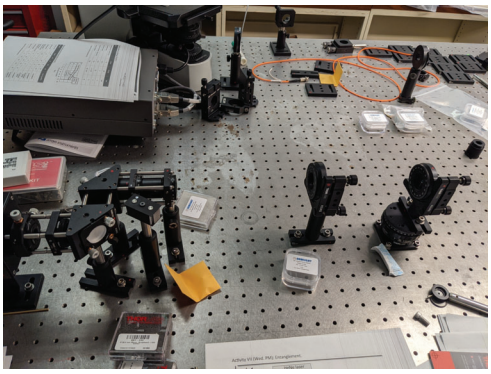

FIG. 4: The 'state generation' portion of the apparatus. The front-end that consists of the collimation setup followed by the birefringent plate and the *DC* crystals. Each individual *DC* crystal facilitates *SPDC*, and orienting them orthogonal to one another in combination with the *BP* generates the desired entangled state.

D. Detecting Entangled Photons

The detection portion of this apparatus consists of two half-wave plates, two polarizing beam splitters, and four single photon avalanche photodiodes (SPAPDs), shown in Figure 5. The detectors take the collected light and send it via optical fibers to four SPAPD modules. These devices are specially constructed silicon photodiodes with a high voltage such that the absorption of a single photon will result in a voltage pulse at the detection electrons, allowing us to detect single photons. The modules we use are produced by Excelitas and have an average dark count of less than 1000 counts per second. The avalanche photodiodes will produce a voltage pulse every time they detect a photon, and these pulses happen very quickly, in less than a nanosecond. This is such a short time interval that in order to detect and calculate how many photons we are getting in each detector, we have to be able to distinguish when we count pairs of photons at the same time in a very small coincidence window. We achieve this via a field programmable gate array coincidence system purchased from QuTools. This system enables us to view, in real time, the 'singles counts' and the 'coincidence counts' between each channel. The singles counts are how many photons each SPAPD module detects individually in a set time bin. On the other hand, coincidence counts are the number of photon pairs are detected between two detectors. This SPAPD module calculates this by measuring when two detectors each detected a photon within a certain time interval, called the 'coincidence window.' For the sake of our experiment, the time bin is 1 second, and the coincidence window is 10 nanoseconds.

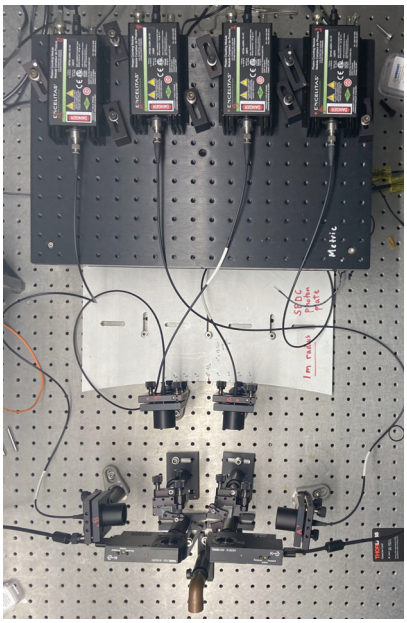

FIG. 5: Image of the detection portion of the apparatus. Consists of two half-wave plates placed in computer-controlled rotation mounts placed along each axis of the resulting beams from the SPDC crystals. Following the half-wave plates are polarizing beam splitters which transmit vertically polarized light and reflect horizontally polarized light to unprimed and primed SPAPDs, respectively.

In order to collect the data and interface with the SPAPDs in a more efficient and accurate manner, we utilize a LabView script that allows me to preset all of the conditions for a trial and then automatically adjusts the automated rotation mounts (with the half-wave plates) and collects the data from the SPAPDs (there is a short discussion of the LabView code in Appendix C). The portion of the LabView front-end I use to set the conditions for a trial is shown in Figure 6.

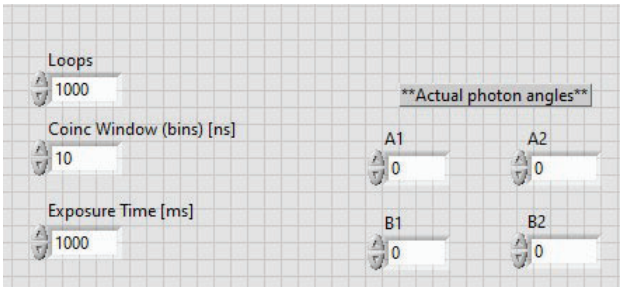

FIG. 6: The portion of the LabView front-end in which I adjust the parameters of the experiment, to include the coincidence window, number of data point taken at each angle pair, and the four angles for a given trial.

Once we have set the parameters for a trial, the code collects and displays data from a QuTau GUI (that is connected to the SPAPD modules) and calculates the relevant values on a different portion of the front-end. An example of what this looks like is shown in Figure 7. This is repeated four times for each expectation value (e.g. $E(\theta_{A1}, \theta_{B1})$, $E(\theta_{A1}, \theta_{B2})$, $E(\theta_{A2}, \theta_{B1})$, and $E(\theta_{A2}, \theta_{B2})$. These four expectation values are then used to calculate S in accordance with the previous theory from Equation (7).

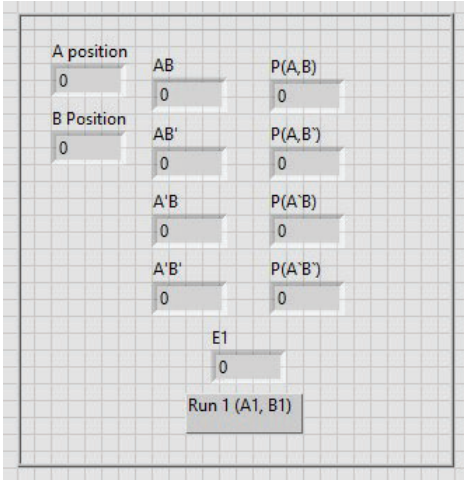

FIG. 7: The LabView front-end for a single angle pair which displays the relevant information for a calculation of the expectation value and joint probabilities.

For the CHSH inequality, we are primarily interested in the expectation value, but we use the other parameters to ensure that the apparatus is going to the correct angle settings, and we also use it to analyze any sources of error.

E. Results and Analysis

The expectation values from Equation (7) are calculated experimentally in terms of the coincidence counts from the four SPAPDs using the following equation:

$$E(\theta_A, \theta_B) = \frac{N_{AB} + N_{A'B'} - N_{A'B} - N_{AB'}}{N_{AB} + N_{A'B'} + N_{A'B} + N_{AB'}} \tag{14}$$

Subsequently, setting the four angles to the maximal violation parameters that, in accordance with quantum theory, yield a maximum violation of the CHSH inequality ($\theta_{A1} = 0°,\ \theta_{A2} = 45°,\ \theta_{B1} = 22.5°,\ \theta_{B2} = -22.5°$), we get the following expectation values:

$$E(0°, 22.5°) = 0.887 \pm 0.008$$
$$E(45°, 22.5°) = 0.80 \pm 0.01$$
$$E(45°, -22.5°) = -0.15 \pm 0.02$$
$$E(0°, -22.5°) = 0.906 \pm 0.008$$

The error bars associated with these expectation values demonstrate the accuracy of the experiment. These particular error bars were calculated using 100 data points at each angle setting and standard error analysis in accordance with a Poisson distribution. These expectation values gave a 'local realism' quantity of:

$$S = 2.75 \pm 0.03 \tag{15}$$

This value demonstrates a clear violation of the CHSH inequality – and thus local realism – and therefore invalidates local hidden variable theory as a means to account for the non-classical behavior of quantum systems. While a value of $S > 2$ when calculating the CHSH inequality is an absolute statement of the violation of local realism, there is some deviation from the theoretically expected values in our experiment, indicated systematic errors in the apparatus used to measure this entangled state. An in-depth analysis of the potential systematic errors is provided in Section IV.

IV. CHARACTERIZING THE APPARATUS

The error with our calculations from the CHSH test of local realism in Section III seemed to be purely statistical noise, and as long as we had a significant number of data points, we were able to reduce the error bars as much

as possible. However, there were deviations from the theoretical predictions of quantum mechanics, so we looked at different relationships in the system in order to assess the accuracy of this apparatus.

The first relationship we analyzed was that from Equation (10) in order to see if there was a sinusoidal relationship between the expectation value and relative angle of half-wave plates A and B. Again, the relationship between expectation value and the angle parameters is given by

$$E(\theta_A, \theta_B) = \cos 2(\theta_A - \theta_B) \tag{16}$$

Figures 8 and 9 show the results, and although the experimental data does not perfectly fit the predicted curve, there is a sinusoidal trend. Figure 9 also shows a periodic trend, indicating that the half-wave plates do not have any significant beam walking that would affect data should the half-wave plate rotate too many times in one direction.

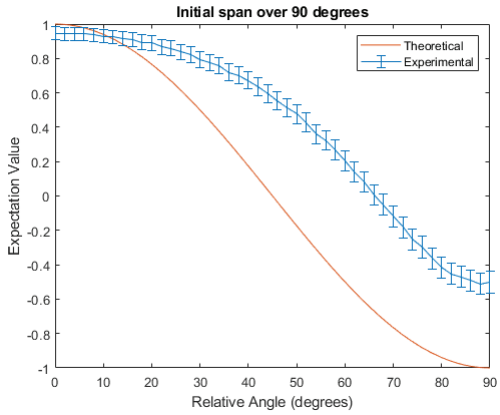

FIG. 8: Graph of the expectation value, $E(\theta_A, \theta_B)$. The red line corresponds to the theoretical prediction of how the expectation value would change as a function of relative angle, as discussed in Aspect's paper [2]. The blue curve is our data with error bars, taken from ten data points at intervals of 2°.

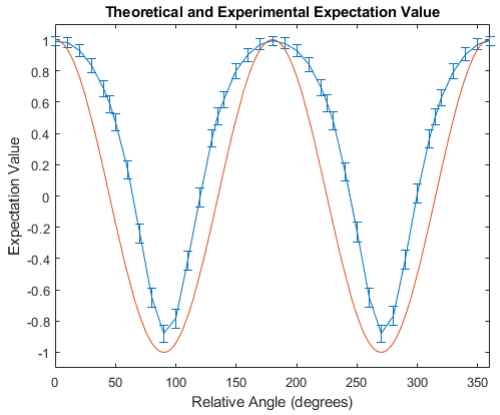

FIG. 9: Graph of $E(\theta_A, \theta_B)$ over a relative angle span of [0°, 360°]. As in Figure 8, the red line corresponds to the theoretical expectation value and the blue line is our data. The general trend follows the expected curve, but there is some observed deviation from the theoretical values.

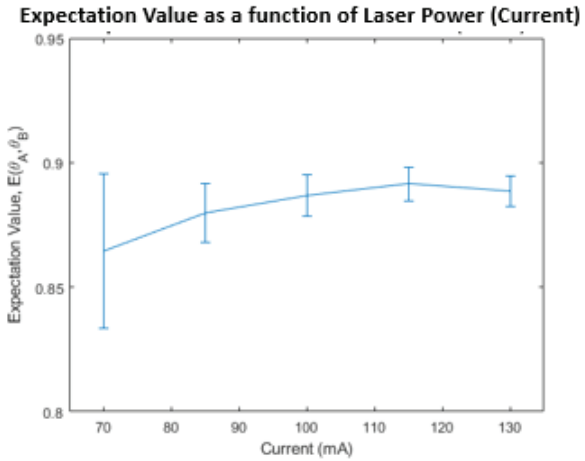

FIG. 10: A graph of the expectation value when the power of the laser is adjusted. The current is adjusted from 70 mA to 130 mA in increments of 15 mA and calculated the expectation value at ($\theta_A = 0°$, $\theta_B = 22.5°$).

It is also possible that, because spontaneous parametric downconversion is a non-linear optical effect, the power supplied to the laser could have an impact on the number of entangled photons that are generated from the downconversion crystals. A graph of this relationship is shown in Figure 10, and because all of the data points are within error bars of one another, it is reasonable to conclude that there is no effect on data calculated for tests of local realism from the power supplied to the laser.

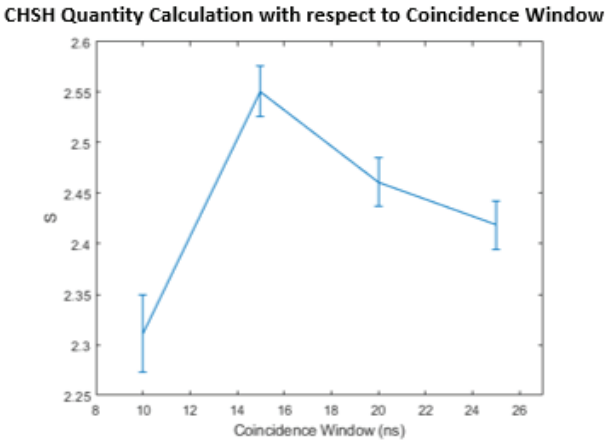

FIG. 11: Graph of the quantity S calculated at the angles ($\theta_{A1} = 0°$, $\theta_{A2} = 45°$, $\theta_{B1} = 22.5°$, $\theta_{B2} = -22.5°$) as adjustments are made to the size of the coincidence window.

Lastly, we looked at whether the size of the coincidence window had any impact at all on the calculation of S. We ran four trials with coincidence window sizes of 10 ns, 15 ns, 20 ns, and 25 ns. The calculations of S were made at the following angles: $\theta_{A1} = 0°$, $\theta_{A2} = 45°$, $\theta_{B1} = 22.5°$, $\theta_{B2} = -22.5°$. There is no trend as a result of adjusting the coincidence window, from Figure 11, but it is significant that all data points were greater than 2, meaning all of the runs violated the CHSH inequality even with these adjustments.

V. THE HARDY TEST

Our previous results indicate a violation of local realism in Section III with respect to the CHSH inequality. There is a second independent test of local realism that is theoretically similar to the CHSH experiment. Having two independent tests would confirm that this apparatus is properly generating entanglement and that it is capable of generating a variety of polarization entangled states.

A. Theory of the Hardy Test

Another test of local realism, which is similar to the Clauser-Horne-Shimony-Holt test, is the Hardy test. We start with a slightly different, but mathematically equivalent, variation of the CHSH inequality:

$$P(\theta_{A1}, \theta_{B1}) \leq P(\theta_{A2}, \theta_{B2}) + P(\theta_{A1}, \theta_{B2}^{\perp}) + P(\theta_{A2}^{\perp}, \theta_{B1}) \tag{17}$$

In the above inequality, as in the CHSH inequality, $\theta^{\perp} = \theta \pm 90°$; it is the perpendicular polarization axis to the axis measured by θ, signifying the primed detector (e.g. A' or B'). Again, if local hidden variable theory is a viable method to account for the results of measurements on entangled states, then the inequality will always be valid. Different from the CHSH test of local realism, we analyze the following entangled state:

$$|\psi_1\rangle = \sqrt{0.2}\,|H\rangle_A\,|H\rangle_B + \sqrt{0.8}\,|V\rangle_A\,|V\rangle_B \tag{18}$$

With this state in mind, the measurement angles that will generate a violation of the inequality in Equation (17) are: $\pm\alpha$ and $\pm\beta$, where $\alpha = 35°$ and $\beta = 19°$. Utilizing these angles, the inequality in Equation (17) is given as

$$P(\beta, -\beta) \leq P(\alpha, -\alpha) + P(\beta, \alpha^{\perp}) + P(-\alpha^{\perp}, -\beta) \tag{19}$$

Subtracting the three terms on the right side of Equation (19), we can define the quantity H in Equation (20) and subsequently define the inequality in terms of only H:

$$H \equiv P(\beta, -\beta) - P(\alpha, -\alpha) - P(\beta, \alpha^{\perp}) - P(-\alpha^{\perp}, -\beta) \leq 0 \tag{20}$$

Therefore, in accordance with local realism theory, $H \leq 0$. Again, this inequality is based in the assumption that, should local hidden variable theory be a viable explanation for the correlation observed in entangled states (i.e. are local hidden variables present when measuring entanglement). However, if $H > 0$, then local realism is violated and there are no hidden variables accounting for a correlation in measurements on an entangled system.

B. Experimental Methods

The Hardy test is very similar to the CHSH inequality test with respect to setup. The key difference is that the maximum violation of local realism occurs with different entangled states:

$$|\psi_1\rangle = \sqrt{0.2}\,|H\rangle_A\,|H\rangle_B + \sqrt{0.8}\,|V\rangle_A\,|V\rangle_B \tag{21}$$

$$|\psi_2\rangle = \sqrt{0.8}\,|H\rangle_A\,|H\rangle_B + \sqrt{0.2}\,|V\rangle_A\,|V\rangle_B \tag{22}$$

For the sake of this experimental analysis, we generated the state $|\psi_1\rangle$, for which the respective angle parameters are $\alpha = 35°$ and $\beta = 19°$. In order to generate this state, we used the exact same apparatus from Figure 2 and the LabView code and front-end in Figures 6 and 7. We placed the back-end half-wave plates (A and B) to 0° and then adjusted the front half-wave plate to get the coincidence counts in the AB and $A'B'$ detector pairs to have a ratio of 1:4. Then, we placed the back-end half-wave plates to $-35°$ and 35° and adjusted the birefringent plate to minimize the 'cross coincidences' (AB' and $A'B$); although they were not zero, they were extremely low relative to the number of coincidence counts in the other detector pairs.

Once the entangled state $|\psi_1\rangle$ was properly generated, I ran four trials, similar to the CHSH test, in order to find the following probabilities:

$$P(\beta, -\beta);\ P(-\alpha, \alpha);\ P(\beta, \alpha^{\perp});\ P(-\alpha^{\perp}, -\beta) \tag{23}$$

C. Analysis of the Hardy Test

Instead of calculating and using expectation values to determine the 'local realism' quantity (as in the CHSH test of local realism), the Hardy test deals only with the probability calculations of one set of coincidence counts per angle setting. These probabilities are calculated below; for the sake of simplicity, we will define the following quantity: $N_{total} = N_{AB} + N_{AB'} + N_{A'B} + N_{A'B'}$. This gives the relevant probabilities for the Hardy test as follows:

$$P(\beta, -\beta) = \frac{N_{AB}}{N_{total}};\ P(-\alpha, \alpha) = \frac{N_{AB}}{N_{total}};$$
$$P(\beta, \alpha^{\perp}) = \frac{N_{AB'}}{N_{total}};\ P(-\alpha^{\perp}, -\beta) = \frac{N_{A'B}}{N_{total}}$$

The results from the most definitive trial in the experiment give the probabilities below:

$$P(\beta, -\beta) = P_{AB}(19^{\circ}, -19^{\circ}) = 0.174 \pm 0.006$$
$$P(-\alpha, \alpha) = P_{AB}(-35^{\circ}, 35^{\circ}) = 0.115 \pm 0.007$$
$$P(\beta, \alpha^{\perp}) = P_{AB'}(19^{\circ}, 35^{\circ}) = 0.014 \pm 0.002$$
$$P(-\alpha^{\perp}, -\beta) = P_{A'B}(-35^{\circ}, -19^{\circ}) = 0.024 \pm 0.002$$

These probabilities yield a result of

$$H = 0.022 \pm 0.009 \tag{24}$$

This result further verifies that quantum mechanics does not adhere to local realism, and this further validates that we are properly generating and measuring an entangled state with my apparatus. The error analysis done on these measurements is the same as that done with the results from the CHSH test.

VI. FURTHER APPLICATIONS OF APPARATUS AND EXPERIMENTATION

One important consideration for this project is the potential exploration into various applications of quantum information science. Of particular interest are applications in quantum computing and quantum cryptography. Although this apparatus does not have single-photon detection fidelity, it has the potential, with some modifications, to be used to conduct a demonstration of quantum cryptography, more specifically quantum key distribution (QKD). An example of QKD is the BB84 protocol, which is a method of generating a cryptographic key utilizing an entangled state for which the resulting key is entirely secure with respect to any third-party entity. This has significant implications in terms of military applications, and a demonstration at the Naval Academy would be a tremendous achievement with respect to the quality of undergraduate research at USNA. There has already been a project developed by a senior from the class of 2023 in cooperation with this project to develop a lab regarding local realism and the CHSH inequality for undergraduate physics majors. A more in-depth discussion of this can be found in Appendix B (Undergraduate Lab Development).

VII. CONCLUSION

Quantum information processing and the technologies around quantum information have critical applications around national security including quantum computing and QKD, and the importance of these concepts has been reinforced by the winning of the Nobel Prize in Physics last year by physicists working in quantum foundations. Hands-on demonstrations of the non-classical aspects of quantum mechanics have been difficult to achieve at the undergraduate level, with institutions like the Naval Academy understanding the significance of these ideas but not having the resources to experimentally explore them. This project has built and validated the first entangled photon source at the United States Naval Academy, and we refined the system and analyzed its behavior over the course of this year. The validation of our apparatus through two independent tests of local realism (the CHSH test and the Hardy test) verifies that we are properly generating entangled states and accurately measuring them, laying the foundation upon which we can begin to venture from demonstrations of the non-locality of quantum mechanics to applications of

entanglement and quantum systems. Furthermore, by developing these laboratory tools at USNA, we have provided the template for advancing quantum information processing at other engineering undergraduate institutions. We continue to hope that this project will lead to future laboratory demonstrations across disciplines, including physics, cyber, and electrical engineering.

---

[1] J. F. Clauser, M. A. Horne, A. Shimony, and R. A. Holt, Physical Review Letters **25**, 880 (1969).
[2] A. Aspect, P. Grangier, and R. Gerard, Physical Review Letters **49**, 91 (1982).
[3] A. Einstein, B. Podolsky, and N. Rosen, Phys. Rev. **47**, 777 (1935).
[4] D. Bohm, *Quantum Theory* (Prentice-Hall, 1951).
[5] J. S. Bell, Physics Physique Fizika **1**, 195 (1964).
[6] M. Beck, *Quantum Mechanics: Theory and Experiment* (Oxford University Press, 2012), ISBN 9780199798230.
[7] L. Maccone, American Journal of Physics **81** (2013).

VIII. APPENDICES

A. Derivation of Bell's Inequality

In his 1964 paper, John Bell addressed the assertion that local hidden variable theory was a viable method for accounting for the correlation seen in quantum systems, particularly entangled systems [5]. Beginning with a pair of spin-$\frac{1}{2}$ particles (simply put: particles that have one of two states along a measurement axis – up or down) that are entangled such that if particle one is measured to be spin 'up,' particle two is measured to be spin 'down.' We can denote the spin of particle one as σ_1 and the spin of particle two as σ_2. A measurement of the spin along an axis, represented by the unit vector $\vec{a}$, will yield a value of ± 1 (e.g., $\vec{\sigma_1} \cdot \vec{a} = \pm 1$).

Making the assumption that there are 'local hidden variables' accounting for any measurement made on particle one or particle two, we can account for these with a single parameter λ. Thus, a measurement outcome of particle one and particle two is a function only of the axis along which a measurement is made and the 'hidden variables.' We can account for both as follows:

$$A(\vec{a}, \lambda) = \pm 1,\ B(\vec{b}, \lambda) = \pm 1 \tag{25}$$

where A and B are the measurements we are making along the axes $\vec{a}$ and $\vec{b}$. By accounting for hidden variables with the parameter λ, we can denote the probability distribution of these hidden variables as $\rho(\lambda)$, which signifies the probability of measuring these hidden variables across a certain range. Implementing this to the expectation value of measurements made on A and B (or the expectation value of the product of the components ($\vec{\sigma_1} \cdot \vec{a}$ and $\vec{\sigma_2} \cdot \vec{b}$)), we get:

$$E(\vec{a}, \vec{b}) = \int A(\vec{a}, \lambda)\, B(\vec{b}, \lambda)\, \rho(\lambda)\, d\lambda \tag{26}$$

The quantum mechanical expectation value, which should be the same as the one represented in Equation (26), is represented as:

$$\langle \vec{\sigma_1} \cdot \vec{a}\ \ \vec{\sigma_2} \cdot \vec{b} \rangle = -\vec{a} \cdot \vec{b} \tag{27}$$

The illustration that this inequality must hold if local hidden variables are accounting for any of the observed quantum mechanical behaviors begins with recognizing that $\rho(\lambda)$must by a normalized probability distribution in Equation (28) (meaning that these hidden variables exist at some point over all space) and that E from Equation (26) is -1 if $\vec{a} = \vec{b}$ only if Equation (29) is true:

$$\int \rho(\lambda) d\lambda = 1 \tag{28}$$

$$A(\vec{a}, \lambda) = -B(\vec{a}, \lambda) \tag{29}$$

Assuming the above two parameters, we can rewrite Equation (26) as

$$E(\vec{a}, \vec{b}) = -\int A(\vec{a}, \lambda)\, A(\vec{b}, \lambda)\, \rho(\lambda)\, d\lambda \tag{30}$$

We can then introduce another unit vector, $\vec{c}$, which we use to measure B and look at the difference in expectation value:

$$\left| E(\vec{a}, \vec{b}) - E(\vec{a}, \vec{c}) \right| \leq -\int \left[1 - A(\vec{b}, \lambda)\, A(\vec{c}, \lambda) \right]\, \rho(\lambda)\, d\lambda \tag{31}$$

The second term in the integrand of Equation (31) is simply $E(\vec{b}, \vec{c})$, giving the following simplification:

$$\left| E(\vec{a}, \vec{b}) - E(\vec{a}, \vec{c}) \right| \leq 1 + E(\vec{b}, \vec{c}) \tag{32}$$

The above form of Bell's inequality is the same as the one presented in Equation (1) in Section II [5].

B. Undergraduate Lab Development

An objective of this project in the initial stages of the proposal was to develop a series of interdisciplinary, undergraduate labs for students at the United States Naval Academy to perform in order to better understand the fundamental concepts in quantum foundations and the relevant applications of quantum information science. I worked with MIDN 1/C Eddie Paz and my other research advisors to develop an initial lab for students regarding entangled systems and the CHSH inequality. The title of MIDN Paz's capstone project is titled: "Development of an Undergraduate Lab using the USNA Entangled Photon Setup." This lab utilizes the entanglement apparatus built by this Trident project and introduces undergraduate physics majors to the concepts of local realism, hidden variable theory, and violations of these principles in accordance with quantum mechanics.

The lab walks students through generating an entangled state with the apparatus in this project as well as measuring various entangled states. In order to drive home the idea of local realism, students can generate purely horizontal states ($|\psi_1\rangle = |H\rangle\,|H\rangle$) and purely vertical states ($|\psi_2\rangle = |V\rangle\,|V\rangle$) and make measurements on those mixed states to understand how the states are being detected and measured. This enables students to learn about not only entanglement, but also optics, as they will have the ability to observe how rotating the half-wave plates adjusts which detectors the down-converted photons are traveling to as they adjust the half-wave plates. Then, students can place the system in a superposition of horizontally and vertically polarized light and learn how to measure these states through the process of ultimately conducting a violation of local realism.

The manual will require some slight modification in order to be properly implemented at the U.S. Naval Academy, but this capstone project, in conjunction with my Trident project, have provided a foundation upon which future labs can be created, both for physics majors alone as well as for interdisciplinary labs and projects for physics, computer engineering, and electrical engineering students.

C. LabView Code

One of the most challenging aspects of this project was installing the back-end equipment and connected software to accurately collect large amounts of data. Of particular concern is the half-wave plates in the detection portion of the apparatus that is discussed in great detail in Section III(D). The purpose of these half-wave plates is to adjust the probability of each detector receiving photons from the generated entangled state. At the beginning of this project, we had manual mounts, similar to the one at the front of the apparatus (in the light collimation portion of the apparatus), shown in Figure 12. These allowed us to adjust the half-wave plates to the appropriate parameters and resulted in us calculating an initial violation of the CHSH test of local realism, but the results had larger error bars and were not very close to the theoretically expected value at the respective parameters.

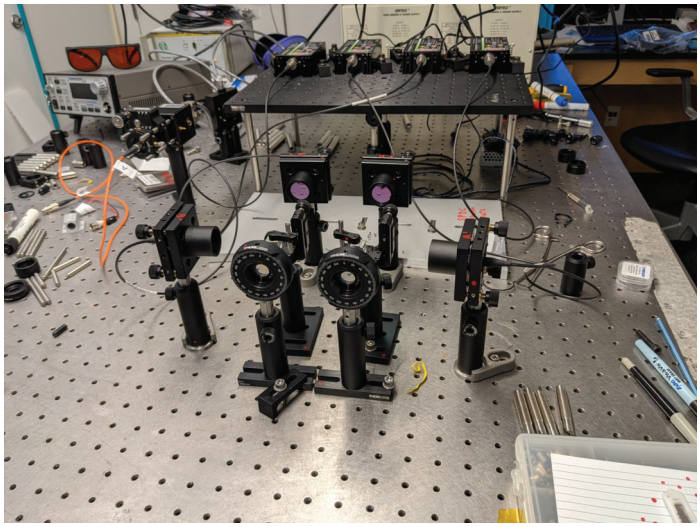

FIG. 12: Image of the half-wave plate rotation mounts from August 2022. These were used to adjust the optical parameters of the downconverted light in the detection portion of the experimental apparatus.

To address this, we added in computer-controlled automated rotation mounts purchased from Thorlabs, shown in Figure 13. These allowed for higher fidelity adjustments of the half-wave plates which in turn allowed us to collect more accurate data and make more precise measurements of the entangled photons.

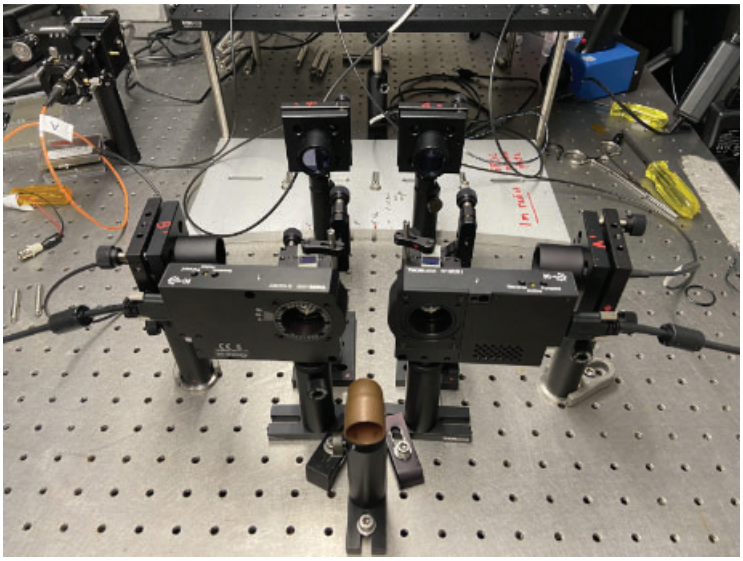

FIG. 13: Image of the computer-controlled rotation mounts that contain the half-wave plates on the detection portion of the experimental apparatus discussed in detail in Section III(D).

These computer-controlled rotation mounts are connected to a computer program that we can connect to LabView in order to design and utilize code that is specific to the experiments we were running. The desired front-end was one that a user could simply input the relevant parameters (e.g. number of data points, coincidence window, time bin, angles, etc.) and then receive all the relevant data to a test of local realism. The final version is shown in Figure 14.

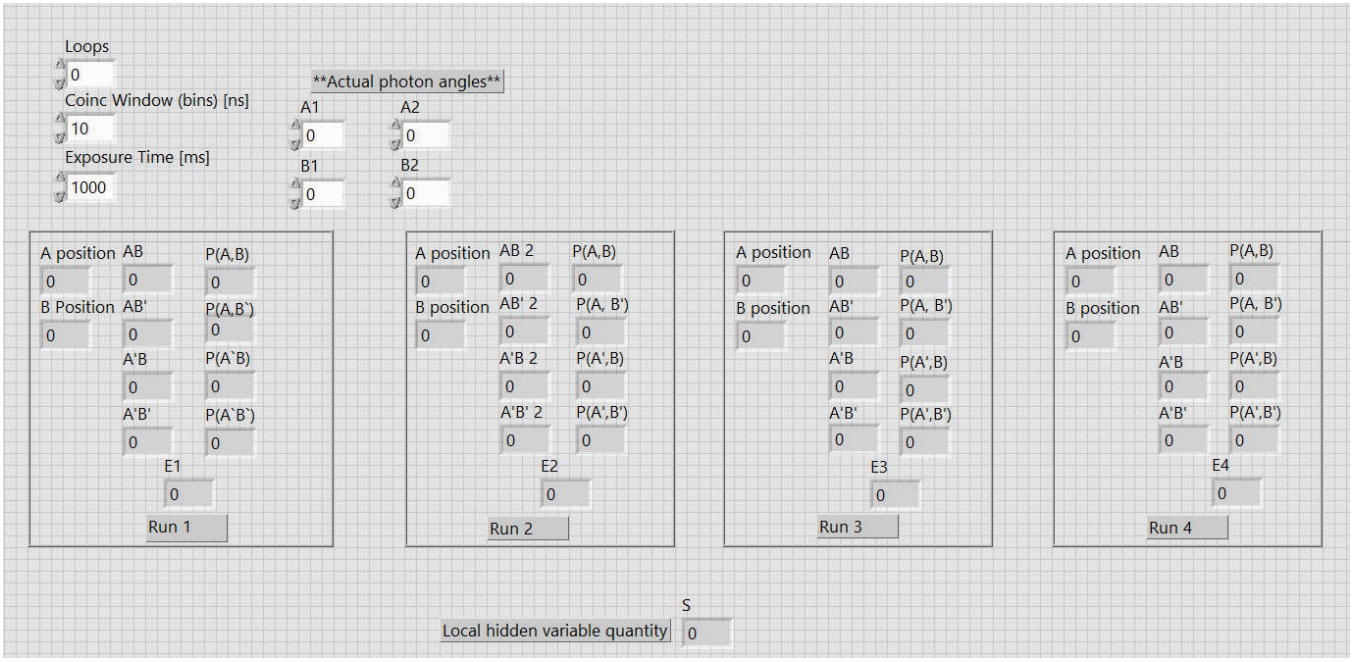

FIG. 14: Image of the LabView front-end used to initialize and conduct measurements on the generated entangled state. Brief description of each parameter: 'Loops' is the number of data points at each angle pair (i.e. each box); 'Coinc Window' sets the size of the coincidence window to calculate coincidence counts in nanoseconds (e.g. 10 nanoseconds); 'Exposure Time' is the overall time bin we sum the coincidence counts in milliseconds (e.g. 1000 is 1 second); 'A1' is the first angle for the A half-wave plate (likewise for 'A2,' 'B1,' and 'B2' with 'B1' and 'B2' corresponding to the B half-wave plate).

The parameters a user can input on the LabView front end shown in Figure 14 are: the number of data points ('Loops'), the coincidence window ('Coinc Window' in nanoseconds), the time bin ('Exposure Time' in milliseconds), and the half-wave plate angles ('A1,' 'B1,' 'A2,' and 'B2'). Once these are put in, a user can click 'Run' and will receive all of the data and calculations on the rest of the front end (in the boxes titled 'Run 1,' 'Run 2,' 'Run 3,' and 'Run 4'), and there is also a portion of the code that automatically feeds the raw data to a file path within the desktop on which this code is saved.

As for what some of the code looks like, portions of this code are shown in Figures 15-18. Figure 15 shows the low-level code associated with taking the half-wave plate positions that a user input (e.g. 'A1' and 'B1' for Run 1) and sends those values to the motor. There is a Boolean condition to account for the fact that (a) rotation mounts are facing different directions (so for them to move in the same direction, A has to move counterclockwise while B moves clockwise and vice versa), and (b) the LabView code is unable to send negative numbers to the rotation mounts. The Boolean condition accounts for both of those conditions and adjusts the user's input parameters to values that are equivalent for the intended data collection but are values that the code and rotation mounts can adequately utilize (e.g. it changes -30 to 330 for the A half-wave plate rotation mount).

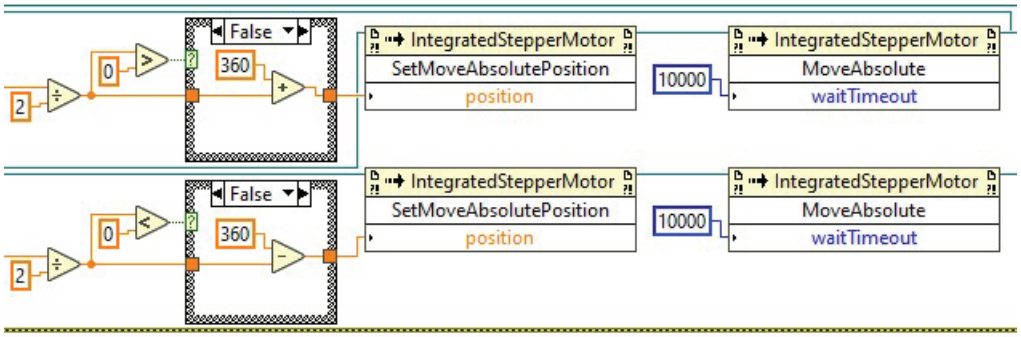

FIG. 15: The LabView code that takes the angles input from the front-end to send to the rotation mounts and in turn rotating the half-wave plates. The Boolean conditions are in place to account for negative values and to account for one of the rotation mounts be placed facing the opposite direction as the other.

Once the input angles have been adjusted and recalculated, the resulting values are sent to the rotation mounts. However, it takes time for the rotation mounts to move to the correct position, and there had been some issues with data collection occuring before the rotation mounts were at the correct position. To prevent this, we placed a 'while' loop in the second frame of Figure 16 that compares the *desired* angle of the rotation mount and the *actual* angle of the rotation mount. The while loop is constructed such that as long as those two angles are different, the code will refrain from moving on to data collection, thereby ensuring that the half-wave plates are at the correct angles before any data is taken.

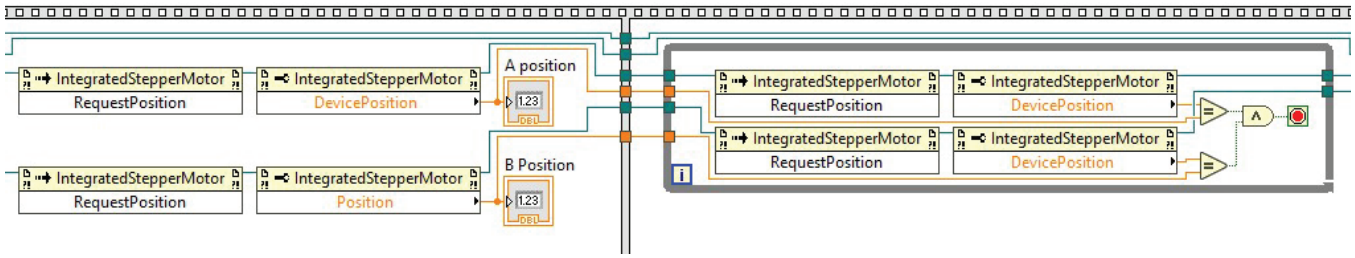

FIG. 16: Image of the LabView code that corresponds to moving the rotation mounts. It takes the values from the Figure 15 and sends it to the rotation mounts, moving them to the desired positions.

The LabView code collects data by connection to the QuTools module and pulling data from there across each time bin. For an actual trial, that means we can calculate how long this will take by multiplying the number of loops (i.e. data points) by the time bin (the 'Time Exposure'), which will give the length of one run in seconds. To collect this data, we had to input the while loop shown in Figure 17, which pulls only the pertinent values for display on the front-end. These important values are the following coincidence counts: N_{AB}, $N_{AB'}$, $N_{A'B}$, and $N_{A'B'}$.

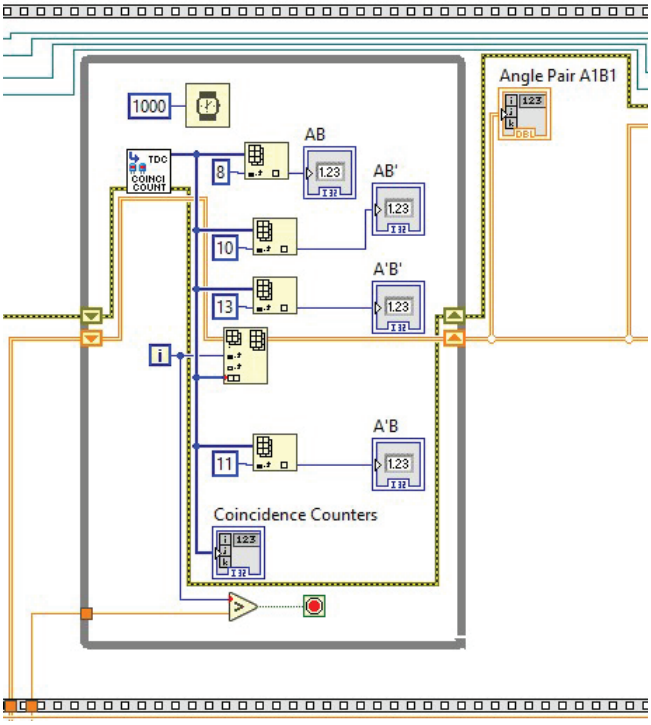

FIG. 17: The code that takes the singles counts and coincidence counts from the QuTools module and displays it on the LabView front end.

Once the data has been displayed on the front-end, the next frame of code, shown in Figure 18, calculates the probabilities and expectation value from the values found in the raw data and then outputs those values in one of the 'Run' boxes in Figure 14. The data is also automatically written and saved to a file with the code shown in the upper-left-hand corner of Figure 18 whose file path is designated at the beginning of the low-level code. Once data from all four angle settings has been collected and the expectation values have been calculated, the last step in the code is to calculate S from the four expectation values and display it at the bottom of the front-end in Figure 14.

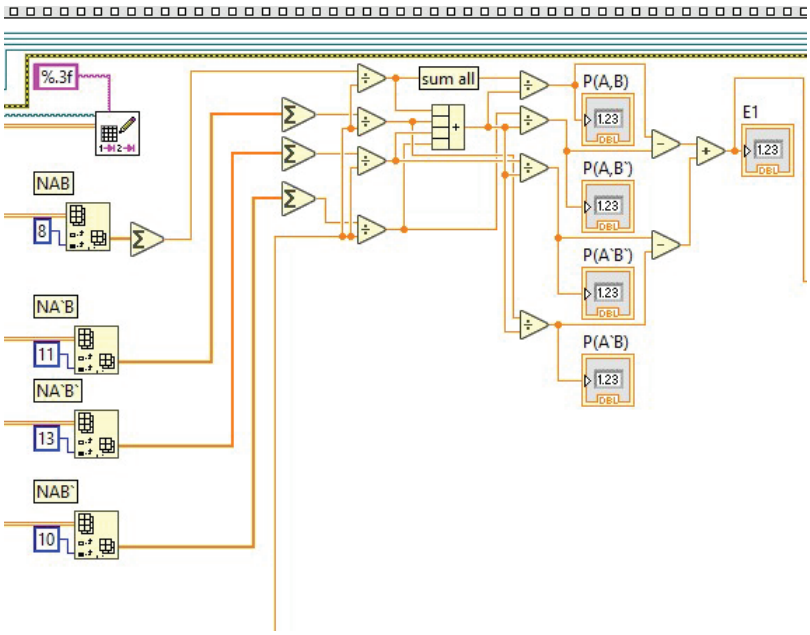

FIG. 18: The LabView code that takes the coincidence counts pulled from the QuTools GUI and calculates the probabilities, expectation values, and ultimately S. It then takes those values and displays them on the LabView front end.